Supplementary Information

Exploring change in the structural integrity of lysozyme in presence of ZnONP: A thermodynamic-based approach

Monalisha Ojha[a], Susmita Mohanta[b], Neeraj Kumar Mishra[c], Sidhartha S. Jena[b], Suman Jha[a*]

[a]Department of Life Science, National Institute of Technology Rourkela, Odisha, 769008, India.

[b]Department of Physics and Astronomy, National Institute of Technology Rourkela, Odisha, 769008, India.

[c]Department of Life Sciences, GITAM School of Science, GITAM deemed to be University, Vishakhapatnam, 530045, AP, India.

Methods:

Moisture content of ZnONP

To measure the moisture content of ZnONP before experimentation, CHNS elemental analysis was performed using an automated Vario EL elemental analyser (Elementar, Germany) showing a hydrogen content of only 0.162 %. This low hydrogen value confirms that occluded or adsorbed water was effectively eliminated during the calcination process. The detailed percentage of C, H, N, and S is give below.

Results

Table ST1: The table shows the weight percentages of carbon (C), hydrogen (H), nitrogen (N), and sulfur (S) in ZnONP. Values are reported as % w/w.

Sample	Weight (mg)	N (%)	C (%)	H (%)	S (%)
ZnONP	5	0.57	0.59	0.162	0.042

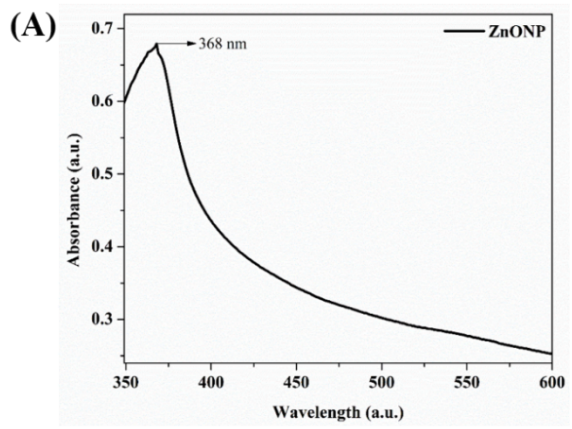

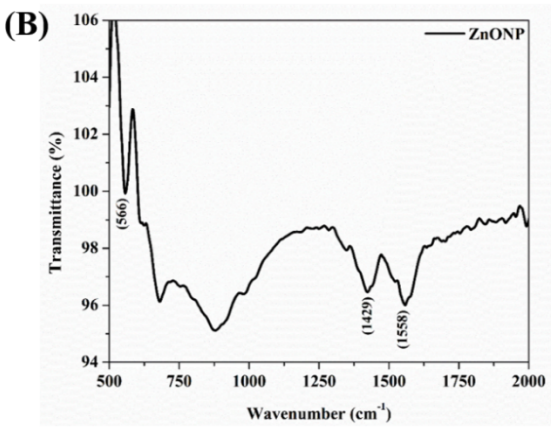

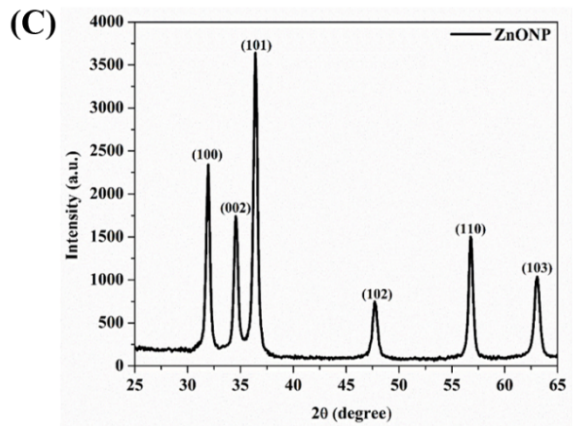

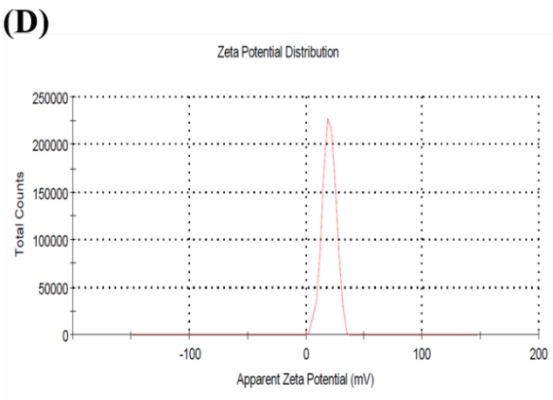

Fig. S1. Characterization of ZnONP. (A) UV-Vis absorption spectrum of ZnONP, (B) ATR-FTIR absorption spectrum showing a characteristic Zn-O stretching, (C) X-Ray diffraction spectrum of ZnONP with characteristic peaks and a crystallite size of 26.5 nm, (D) Zeta potential analysis of ZnONP showing a positive surface charge of 19.9 mV.

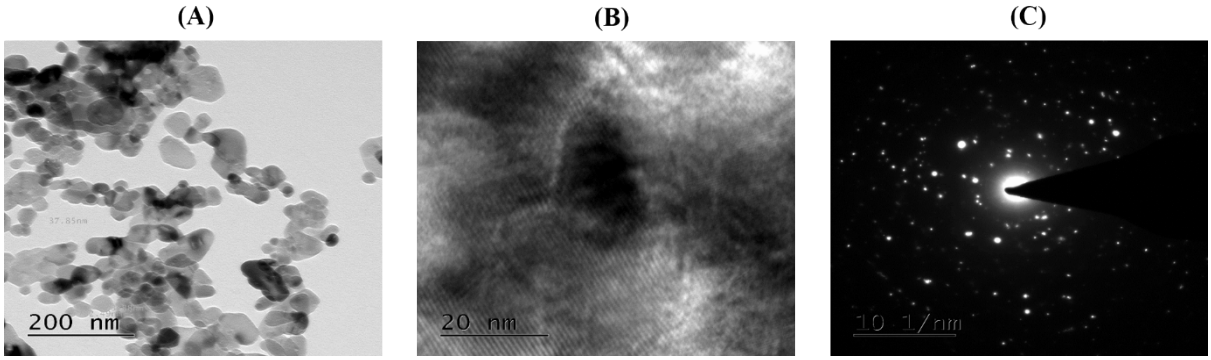

Fig. S2. TEM micrograph showing (A) spherical ZnONP with an average size of 30-40 nm, (B) HR-TEM showing crystal lattice of ZnONP, and (C) SAED pattern of ZnONP.

The above characterization of ZnO nanoparticles (ZnONP) indicates that their properties are similar to those of ZnONP reported in previous studies. Fig. S1. (A) indicates the UV-Vis spectrum of ZnONP with an absorption peak at 368 nm which is the characteristic peak for ZnONP. Further confirmation studies were done using Attenuated Total Reflection-Fourier Transform Infrared (ATR-FTIR) spectroscopy and X-ray diffraction with powdered samples at a range of 500-2000 cm^{-1} and at 2θ range of 25° to 65° at a scan rate of 20°/min and step size of 0.05° respectively. FTIR spectrum (Fig S1. B) shows characteristic bands at 566 cm^{-1}, 1429 cm^{-1} and 1558 cm^{-1} depicting Zn-O bond stretching vibration, asymmetric –COO- vibration and –C-H- bending vibration respectively. While, Zn-O vibrations depicts the presence of ZnONP particles, whereas all other vibrations are attributed to the presence of residual acetate moieties left after the course of synthesis. Similarly, XRD pattern of synthesized ZnONP showed characteristic peaks at 2θ values of 31.89°, 34.58°, 36.37°, 47.76°, 56.77°, and 63° with the crystallographic planes (100), (002), (101), (102), (110), and (103) respectively. The crystallite size was determined to be 26.5 nm using Scherrer's equation. All the data analysis for XRD were done using X'Pert High Score. The diffraction pattern of the synthesized ZnONP was compared against standard reference patterns in the database. Based on the peak similarity and matching scores, the software identified a reference compound with a 98% match (Schulz, H. et. al., 1979, Solid State Communications, v32(9), p783) to ZnO crystalline structure, confirming its identity and purity to 98%. The surface charge of ZnONP

was found to be +19.9 mV by Zeta sizer and the average diameter of these spherical shaped nanoparticles were approximately 30-40 nm on an average as illustrated by TEM micrographs. The crystalline properties of synthesized ZnONP were further evaluated using HR-TEM (High Resolution TEM) and SAED (selected area electron diffraction) pattern. The HR-TEM image clearly shows well reserved lattice fringes which confirms high crystallinity of ZnONP. This is further corroborated by SAED pattern which shows distinct ring like arrangement of particles which is characteristic of crystalline materials. This ring pattern indicates that the ZnONP has numerous randomly oriented crystallites, confirming their polycrystalline nature and the presence of various crystal orientations.

Table. ST2. Experimental details of ITC titration for controls. The table includes the full compositions of titrand (in cell) and titrant (in syringe), and experimental temperature used for titration.

Titrations	pH	Titrand Composition	Titrant Composition	Temperature (K)
A, B	7.4	Phosphate Buffer (10 mM)	Lysozyme (50 μM)	298.15
C, D	7.4	ZnONP (30 μg/mL)	Phosphate Buffer (10 mM)	298.15
E, F	9	Glycine-NaOH Buffer (10 mM)	Lysozyme (50 μM)	298.15
G, H	9	ZnONP (30 μg/mL)	Glycine-NaOH Buffer (10 mM)	298.15

Table ST3: Raw data corresponding to the titration of 10 mM PB and GN in cell whereas, 50 μM Lysozyme was taken in syringe at 298.15 K and $p = 1.0 \times 10^5$ Pa at pH 7.4 & 9 respectively. The syringe was filled with Lysozyme dissolved in PB and GN. Here Lysozyme is added to the sample cell in each titration during the main /ligand titration experiment and $\Delta H°$ is the

enthalpy of dilution and molar ratio is the ratio between concentration of ligand to substrate in each injection.

Injection Number	**Injection Volume (Titrant Volume) (×10−6 L)**	**Molar Ratio (PB/LF) × 10^{-4}**	**ΔH° (kJ/mol) for PB/LF titration**	**Molar Ratio (GN/LF) × 10^{-4}**	**ΔH° (kJ/mol) for GN/LF titration**
1	0.4	0.1	8.2	0.1	-59.6
2	2.0	0.6	-5.8	0.6	-40.0
3	2.0	1.1	-4.9	1.1	-29.6
4	2.0	1.6	27.7	1.6	-49.4
5	2.0	2.1	-14.8	2.1	-19.1
6	2.0	2.6	21.4	2.6	-38.2
7	2.0	3.1	13.3	3.1	-54.7
8	2.0	3.6	34.5	3.6	-33.8
9	2.0	4.1	-1.8	4.1	-33.6
10	2.0	4.6	-7.5	4.6	-21.6
11	2.0	5.1	35.2	5.1	-28.4
12	2.0	5.6	76.3	5.6	-34.6
13	2.0	6.1	-4.4	6.1	-34.4
14	2.0	6.6	-61.3	6.6	-47.4
15	2.0	7.1	-8.2	7.1	-34.9
16	2.0	7.6	28.2	7.6	-28.4
17	2.0	8.1	-29.7	8.1	-28.7
18	2.0	8.6	-19.4	8.6	-34.4
19	2.0	9.1	-55.6	9.1	-19.9

Table ST4: Raw data corresponding to the titration of 30 μg/mL ZnONP dissolved in PB and GN in cell whereas, 10 mM PB and GN was taken in syringe at 298.15 K and p = 1.0 × 10^5 Pa at pH 7.4 & 9 respectively. The syringe was filled with PB and GN. Here buffer is added to the sample cell in each titration during the main /ligand titration experiment and ΔH° is the enthalpy of dilution molar ratio is the ratio between concentration of ligand to substrate in each injection.

Injection Number	Injection Volume (Titrant Volume) (×10−6 L)	Molar Ratio (ZnONP/PB)	ΔH° (kJ/mol) for ZnONP/PB titration	Molar Ratio (ZnONP/GN)	ΔH° (kJ/mol) for ZnONP/GN titration
1	0.4	0.169	-0.526	0.169	1.20217
2	2.0	1.017	-0.072	1.017	-0.05993
3	2.0	1.864	-0.030	1.864	-0.00738
4	2.0	2.712	-0.024	2.712	-0.01874
5	2.0	3.559	-0.031	3.559	-0.0025
6	2.0	4.407	-0.023	4.407	-0.07627
7	2.0	5.254	0.046	5.254	-0.06967
8	2.0	6.102	-0.009	6.102	-0.05052
9	2.0	6.949	-0.030	6.949	-0.05263
10	2.0	7.797	-0.041	7.797	-0.01643
11	2.0	8.644	-0.054	8.644	-0.07667
12	2.0	9.492	-0.022	9.492	-0.08775
13	2.0	10.339	-0.009	10.339	-0.04533
14	2.0	11.186	-0.039	11.186	-0.0783
15	2.0	12.034	-0.003	12.034	-0.06506
16	2.0	12.881	-0.006	12.881	-0.016
17	2.0	13.729	-0.051	13.729	-0.05231

18	2.0	14.576	0.001	14.576	-0.02012
19	2.0	15.424	0.017	15.424	-0.03412

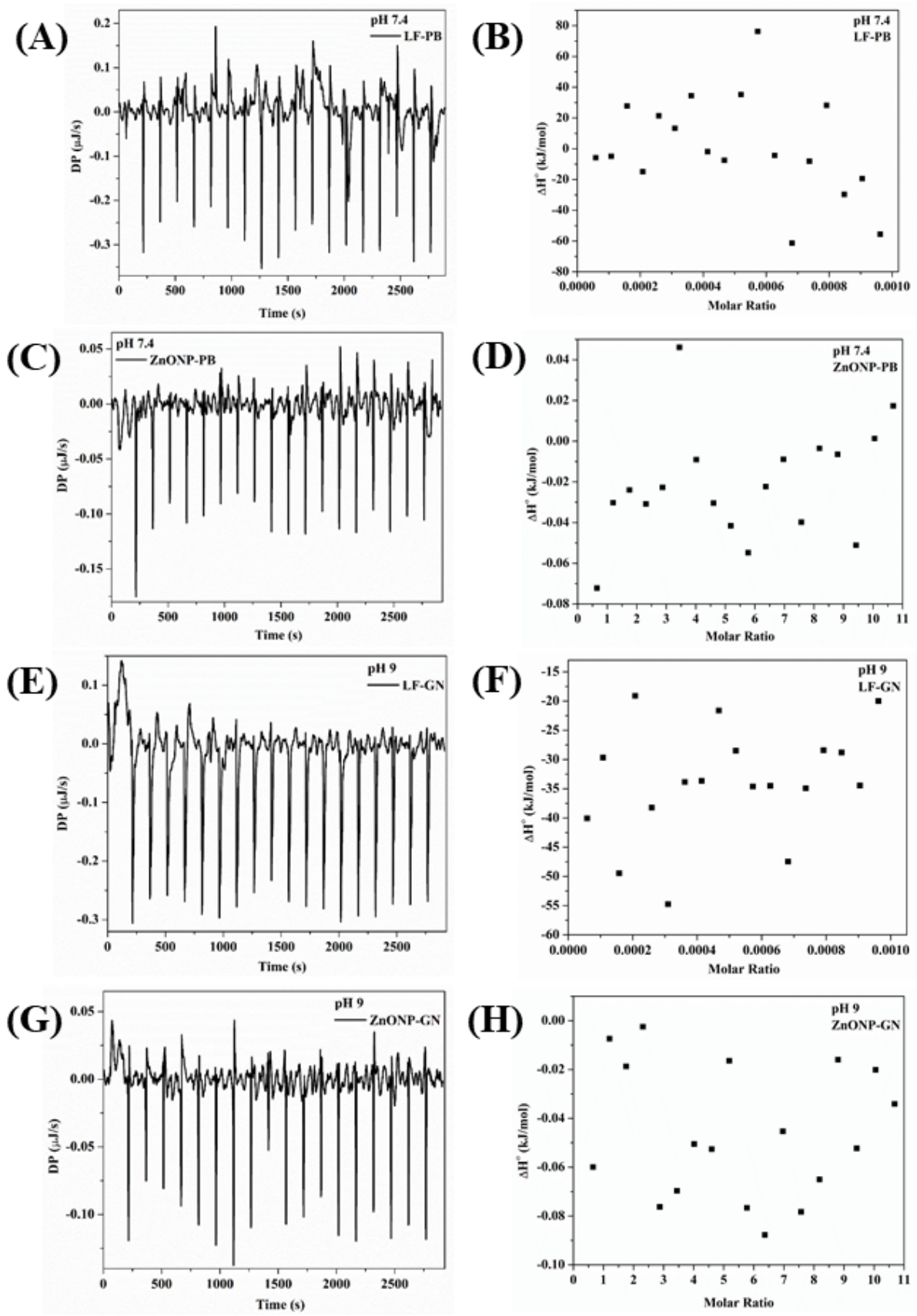

Fig. S3. ITC thermograms of the controls used for baseline correction and calibration.

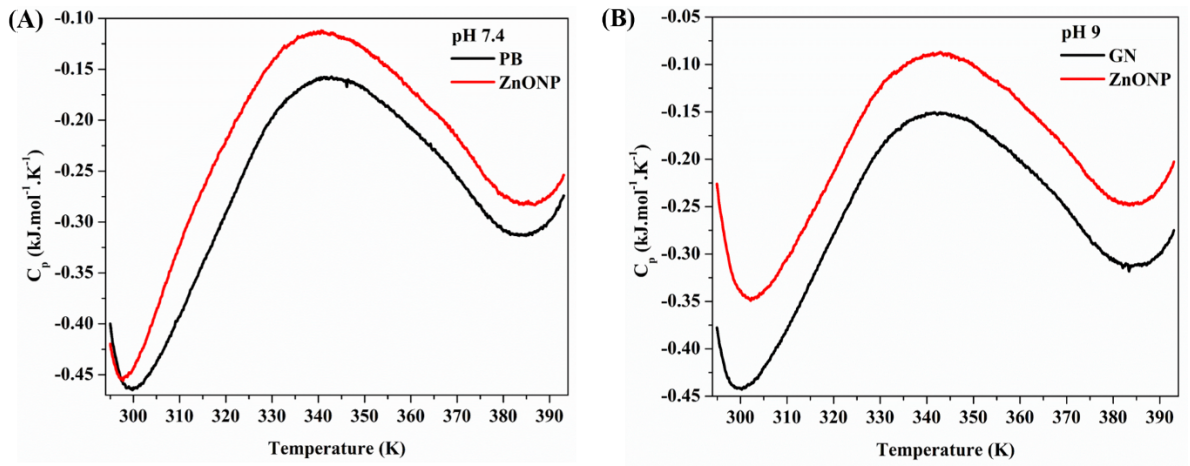

Fig. S4. DSC thermograms of controls, comprising the buffer used for subtraction and ZnONP dissolved in (A) Phosphate buffer, and (B) Glycine-NaOH buffer.

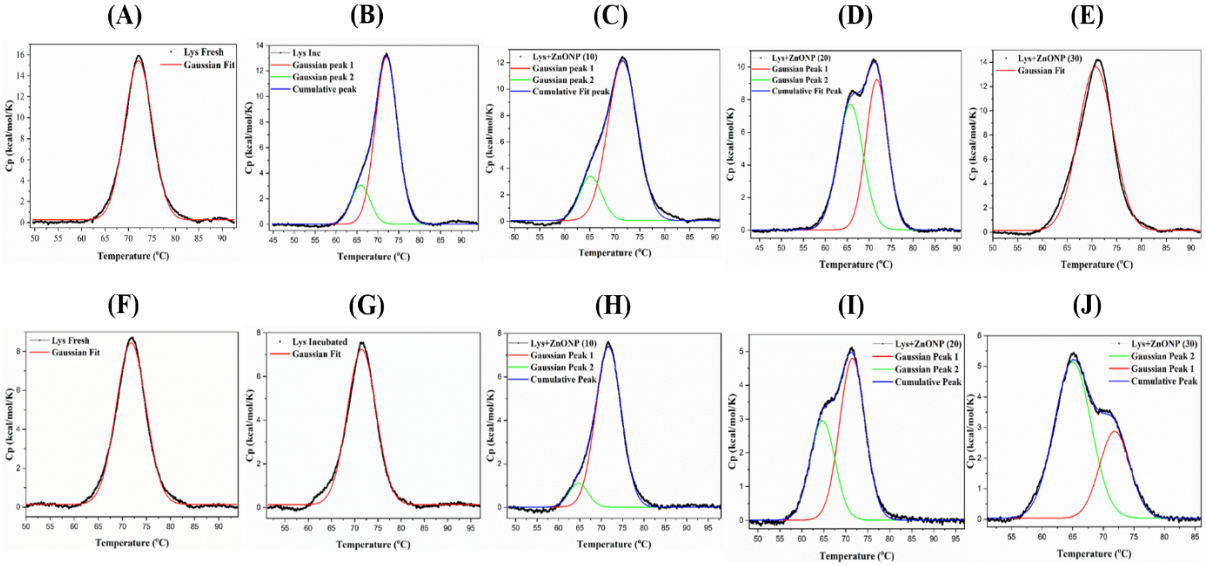

Fig. S5. DSC thermograms of (A) freshly prepared lysozyme (50 µM), (B) lysozyme subjected to a 12-hour incubation and, Lysozyme in the presence of varying concentrations of ZnONP (C) 10 mg/mL (D) 20 mg/mL and (E) 30 mg/mL at pH 7.4. DSC thermograms of (F) freshly synthesized lysozyme (50 µM), (G) lysozyme subjected to a 12-hour incubation and, Lysozyme in the presence of varying concentrations of ZnONP (H) 10 mg/mL (I) 20 mg/mL and (J) 30 mg/mL at pH 9. The graphs were derived by deconvoluting using Origin 8.5 through Gaussian fitting.

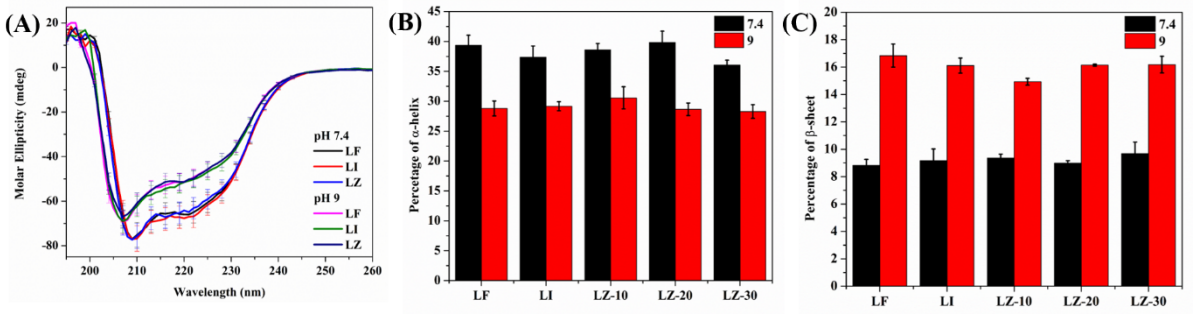

Fig. S6. (A) Far-UV CD spectra of native lysozyme (fresh & incubated) and lysozyme-ZnONP complexes at pH 7.4 and pH 9.0. Percentage of a-helix and b-sheet content in lysozyme and lysozyme-ZnONP complexes at (B) pH 7.4 and (C) pH 9.

The CD spectra for fresh lysozyme at pH 7.4 and 9 are similar with a slight shift in the peak and intensity. The decreased intensity and shifting of peaks can be attributed to unfolding at pH 9 as compared to the protein at pH 7.4. But, in the presence of ZnONP, the CD spectra remain unaltered, contributing to the fact that lysozyme's secondary structure remains unchanged in the presence of ZnONP for both pH values at 298.15 k. These results were also consistent at 338.15 K (data not shown). Further, to investigate the percentage of α-helix and β-sheet, the CD spectra were deconvoluted using the CDNN software tool. There was a considerable decrease in α-helical content in pH 9 as compared to 7.4, and vice-versa for β-sheet. However, as stated previously, the addition of ZnONP does not significantly alter the percentage of neither α-helix nor β-sheet at both the pH conditions.

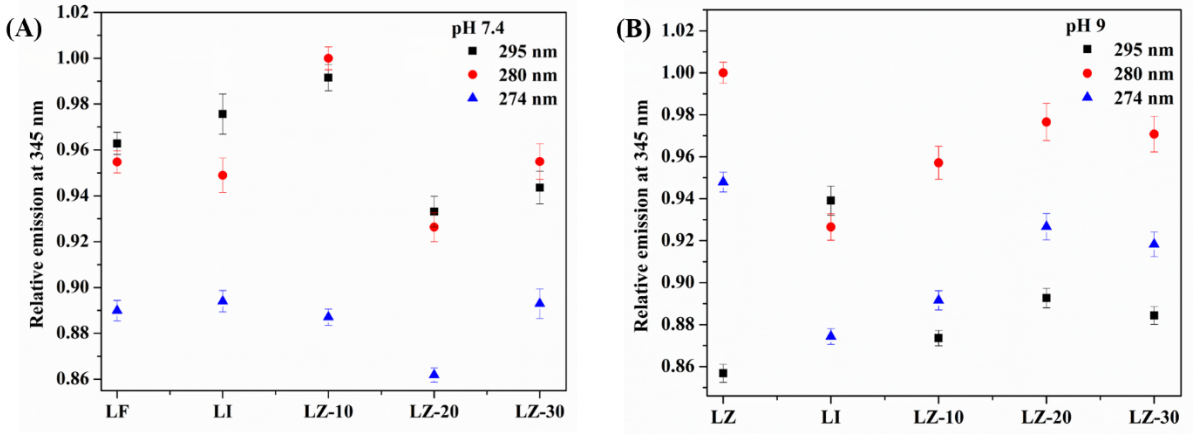

Fig. S7. Steady-state fluorescence emission spectra of lysozyme at pH 7.4 and pH 9. The change in relative emission of lysozyme and lysozyme-ZnONP complexes at (A) pH 7.4 and (B) pH 9 at 345 nm.

Further, to evaluate these findings, steady-state fluorescence of protein in absence and presence of ZnONP for both the pH conditions were measured. Since lysozyme structure has aromatic amino acid in its sequence, i.e., tyrosine, tryptophan and phenylalanine, the fluorescence emission at 345 nm was observed to monitor the changes in the local physicochemical environment, reflecting the tertiary structure of the protein, upon excitation at 274, 280 and 295 nm. At pH 7.4, insignificant change was observed in emission maxima with the addition of ZnONP. A slight increase in emission maxima was noted at lower concentration of ZnONP, but as the ZnONP concentration increased the emission maxima for all three excitation wavelengths dropped down to control value, which suggested insignificant change in the microenvironments of the hydrophobic amino acids. At pH 9, there was a slight reduction in emission maxima at 345 nm for the excitation with 274 and 280 nm, which indicated that lysozyme in presence of ZnONP adapts a rigid structure close to its native conformation at pH 9.

REFERENCES

1. Chakraborti, S., Chatterjee, T., Joshi, P., Poddar, A., Bhattacharyya, B., Singh, S. P., Gupta, V., & Chakrabarti, P. (2010). Structure and activity of lysozyme on binding to ZnO nanoparticles. Langmuir: the ACS journal of surfaces and colloids, 26(5), 3506–3513. https://doi.org/10.1021/la903118c

2. Durowoju, I. B., Bhandal, K. S., Hu, J., Carpick, B., & Kirkitadze, M. (2017). Differential Scanning Calorimetry - A Method for Assessing the Thermal Stability and Conformation of Protein Antigen. Journal of visualized experiments: JoVE, (121), 55262. https://doi.org/10.3791/55262

3. Freire, E., van Osdol, W. W., Mayorga, O. L., & Sanchez-Ruiz, J. M. (1990). Calorimetrically determined dynamics of complex unfolding transitions in proteins. Annual review of biophysics and biophysical chemistry, 19, 159–188. https://doi.org/10.1146/annurev.bb.19.060190.001111

4. Saboury, A. A., & Moosavi-Movahedi, A. A. (1994). Clarification of calorimetric and van't hoff enthalpies for evaluation of protein transition states. Biochemical Education, 22(4), 210-211.

5. Privalov, P. L., & Potekhin, S. A. (1986). [2] Scanning microcalorimetry in studying temperature-induced changes in proteins. In Methods in enzymology (Vol. 131, pp. 4-51). Academic Press.

6. Gorin, G., Wang, S. F., & Papapavlou, L. (1971). Assay of lysozyme by its lytic action on M. lysodeikticus cells. *Analytical biochemistry*, *39*(1), 113–127. https://doi.org/10.1016/0003-2697(71)90467-2

7. Moghadam, T. T., Ranjbar, B., Khajeh, K., Etezad, S. M., Khalifeh, K., & Ganjalikhany, M. R. (2011). Interaction of lysozyme with gold nanorods: conformation and activity investigations. *International journal of biological macromolecules*, *49*(4), 629–636. https://doi.org/10.1016/j.ijbiomac.2011.06.021

8. Das, A., Thakur, R., Dagar, A., & Chakraborty, A. (2014). A spectroscopic investigation and molecular docking study on the interaction of hen egg white lysozyme with liposomes of saturated and unsaturated phosphocholines probed by an anticancer drug ellipticine. *Physical Chemistry Chemical Physics*, *16*(11), 5368-5381.